NMR Studies of Ligand Binding to $P450_{eryF}$ Provides Insight into the Mechanism of Cooperativity†

Arthur G. Roberts,‡ M. Dolores Díaz,‡ Jed N. Lampe,‡ Laura M. Shireman,‡ Jeffrey S. Grinstead,‡ Michael J. Dabrowski,‡ Josh T. Pearson,‡ Michael K. Bowman,§ William M. Atkins,‡ and A. Patricia Campbell*,‡

Department of Medicinal Chemistry, School of Pharmacy, University of Washington, Box 357610, Seattle, Washington 98195, and Structural Biology and Microimaging, Battelle Northwest Laboratories, Richland, Washington 99352-0999

Received September 15, 2005; Revised Manuscript Received December 7, 2005

ABSTRACT: Cytochrome P450's (P450's) catalyze the oxidative metabolism of most drugs and toxins. Although extensive studies have proven that some P450's demonstrate both homotropic and heterotropic cooperativity toward a number of substrates, the mechanistic and molecular details of P450 allostery are still not well-established. Here, we use UV/vis and heteronuclear nuclear magnetic resonance (NMR) spectroscopic techniques to study the mechanism and thermodynamics of the binding of two 9-aminophenanthrene (9-AP) and testosterone (TST) molecules to the erythromycin-metabolizing bacterial $P450_{eryF}$. UV/vis absorbance spectra of $P450_{eryF}$ demonstrated that binding occurs with apparent negative homotropic cooperativity for TST and positive homotropic cooperativity for 9-AP with Hill-equation-derived dissociation constants of $K_S = 4$ and 200 μM, respectively. The broadening and shifting observed in the 2D-{^{1}H,^{15}N}-HSQC-monitored titrations of ^{15}N-Phe-labeled $P450_{eryF}$ with 9-AP and TST indicated binding on intermediate and fast chemical exhange time scales, respectively, which was consistent with the Hill-equation-derived K_S values for these two ligands. Regardless of the type of spectral perturbation observed (broadening for 9-AP and shifting for TST), the ^{15}N-Phe NMR resonances most affected were the same in each titration, suggesting that the two ligands "contact" the same phenylalanines within the active site of $P450_{eryF}$. This finding is in agreement with X-ray crystal structures of bound $P450_{eryF}$ showing different ligands occupying similar active-site niches. Complex spectral behavior was additionally observed for a small collection of resonances in the TST titration, interpreted as multiple binding modes for the low-affinity TST molecule or multiple TST-bound $P450_{eryF}$ conformational substates. A structural and energetic model is presented that combines the energetics and structural aspects of 9-AP and TST binding derived from these observations.

Cytochrome P450's (P450's)[1] catalyze the oxidative metabolism of most drugs and toxins (*2*). Extensive studies with mammalian P450's have shown that a significant subset of these enzymes (3A4 and 2C9) exhibit both homotropic and heterotropic allosteric effects toward a number of substrates (*3*, *4*). These allosteric effects require that multiple substrates or a substrate and an effector be simultaneously bound to the P450. However, the mechanisms by which multiple ligand binding alters rates of individual steps in the P450 reaction cycle are incompletely characterized. The P450 reaction cycle is complex, and in every step of the cycle, local changes in the active site occur and might be connected to the observed cooperativity. Thus, the study of cooperativity in P450's presents a complicated scientific problem but an important one because of the obvious implications that allostery may have in drug−drug interactions and, consequently, for the development of experimental methods able to predict drug incompatibilities.

Established methods used in the study of allostery of P450 metabolism include X-ray crystallography, deuterium kinetic isotope effects, and UV/vis spectroscopy. These methods have provided valuable structural and mechanistic insight into substrate binding (*5*), substrate-dependent heme spin-state change (UV/vis) (*6*), and regioselectivity of substrate oxidation (deuterium effects) (*7*). Solution-state nuclear magnetic resonance (NMR) spectroscopy provides a fourth and novel method for the study of P450 allostery.

NMR offers many advantages over other techniques for the investigation of substrate binding to P450's, because it can provide a dynamic view of the binding process through the mapping of site-specific substrate−protein interactions. NMR spectroscopic techniques are not new to the study of bacterial P450 systems. Titrations of $P450_{CAM}$ against the aromatic alcohol, 2-ethoxyphenol, and cyanide have been followed by ^{1}H NMR, yielding evidence for protein−ligand adducts (*8*). Titrations of $P450_{CAM}$ with aromatic bases have

† This work was supported by National Institutes of Health Grants, GM-32165, and the NIGMS Grant, GM61904, from the WR Wiley Environmental Molecular Sciences Laboratory, a national scientific user facility sponsored by the Department of Energy's Office of Biological and Environmental Research and located at Pacific Northwest National Laboratory.

* To whom correspondence should be addressed. Telephone: (206) 685-2468. Fax: (206) 685-3252. E-mail: apc@u.washington.edu.

‡ University of Washington.

§ Battelle Northwest Laboratories.

[1] Abbreviations: 9-AP, 9-aminophenanthrene; DEB, 6-deoxyerythronolide B, TST, testosterone; NMR, nuclear magnetic resonance; HSQC, heteronuclear single-quantum coherence; P450, cytochrome P450; EPR, electron paramagnetic resonance.

10.1021/bi0518895 CCC: $33.50 © 2006 American Chemical Society
Published on Web 01/19/2006

been investigated with 1D and 2D ^{1}H NMR spectroscopy, providing insight into the structure of the $P450_{CAM}$ ligand-binding site (*9*). In addition, heteronuclear NMR methods have been applied to monitor the formation of the $P450_{CAM}$/putidaredoxin complex, and perturbations in the $P450_{CAM}$ structure upon addition of putidaredoxin have been correlated with the elements that control molecular recognition (*10*). These studies point to the utility of NMR-based techniques for studying P450 allostery.

Whereas the ultimate goal of any NMR study probing P450 allostery is to provide a detailed picture of mammalian P450 metabolism, mammalian cytochrome P450's (denoted as CYP instead of P450) have proven notoriously difficult to solubilize in monomeric forms, at least at the high concentrations required for NMR. Model bacterial systems have therefore been used in their place. $P450_{eryF}$ is a bacterial P450 that shows both excellent solubility and aggregation properties, as well as cooperativity of substrate binding. It has been used as a model for cooperativity in CYP3A4 (*11*−*14*), which is the major drug metabolizing isoform in humans (*15*, *16*). $P450_{eryF}$ metabolizes just one natural substrate (6-deoxyerythronolide B or 6-DEB), but it has been observed to exhibit allosteric behavior in the binding of several ligands, including 9-aminophenanthrene (9-AP), androstenedione, and testosterone (TST) (*5*, *13*, *14*). $P450_{eryF}$ thus constitutes an excellent model P450 system for biophysical and, specifically, NMR analysis. Moreoever, the $P450_{eryF}$ crystal structure is the only X-ray crystal structure of P450 to show two ligands that are bound in the active site (*5*).

Two ligands were selected for analysis: 9-AP, a type-II binder, and TST, a type-I binder (*5*, *13*, *17*). These ligands were selected on the basis of previous studies indicating cooperative binding to $P450_{eryF}$ and X-ray crystal structures demonstrating two ligand molecules bound within the active-site pocket (*5*, *13*, *17*). In addition, 9-AP and TST display substantial differences in affinity for $P450_{eryF}$ (K_S (Hill) = 7.8 μM for 9-AP and K_S (Hill) = 410 μM for TST)[2] (*17*) and exhibit different spin effects on the $P450_{eryF}$ heme environment. 9-AP, a type-II ligand, coordinates directly to the central Fe^{3+} and converts the small amount of high-spin heme in the unliganded P450 to low spin (*13*). In contrast, TST, the type-I ligand, displaces the water that is coordinated to the central Fe^{3+} and shifts the heme to a high-spin state (*17*).

At least two molecules of the ligand, in this study, 9-AP or TST, are believed to occupy the $P450_{eryF}$ active site simultaneously (*5*, *17*). The simplest model for binding of two ligands to $P450_{eryF}$ is the sequential-ordered binding mechanism, shown to be valid for CYP3A4 with TST (*18*, *19*) and shown below for the ligand (L), the first binding constant (K_S), and the second binding constant (αK_S)

$$[P450] \overset{K_S}{\rightleftharpoons} [P450{\cdot}L] \overset{\alpha K_S}{\rightleftharpoons} [P450{\cdot}L{\cdot}L]$$

In our study, UV/vis and NMR-based techniques were combined with computer modeling to delineate the mechanism of homotropic cooperativity of 9-AP and TST for $P450_{eryF}$. Ligand-induced spin states and spin-state equilibria of the P450 heme were probed with UV/vis spectroscopy. Structural and dynamic aspects were probed with NMR. When the sequential-ordered binding model presented above is fit to the ligand-induced changes observed with these spectroscopic techniques, a structural and energetic model for homotropic cooperativity in TST and 9-AP binding to $P450_{eryF}$ could be derived.

MATERIALS AND METHODS

Preparation of the Mutant F86Y. The mutant $P450_{eryF}$ F86Y was made using the QuikChange site-directed mutagenesis kit (Stratagene, La Jolla, CA).

Expression and Purification of ^{15}N-Phe-Labeled and Unlabeled $P450_{eryF}$. The ^{15}N-Phe-labeled $P450_{eryF}$ was expressed using the pTrc99 plasmid system in DL-39, an auxotrophic strain of *Escherichia coli* (tyrB- ilvE- aspC-). Six 50 mL cultures were grown overnight at 37 °C in modified M9 minimal media (Redfield media) supplemented with trace metals, 4% glucose, and ^{15}N-Phe (Cambridge Isotope Labs). These starter cultures were then used to inoculate six 1 L expression cultures. The expression cultures were allowed to continue to incubate at 37 °C until they reached ~1 OD_{600}. At that point, cells were induced by adding IPTG and δ-aminolevulinic acid, each at a stock concentration of 0.5 M, to a final concentration of 1 mM. The incubation temperature was reduced to 30 °C, and the cultures were incubated for a further 24 h, at which time they were harvested.

$P450_{eryF}$ was purified as described previously by ref *20*. The mass was confirmed for the labeled and unlabeled $P450_{eryF}$ by LC/ESI−MS analysis, which was performed on a Micromass Quattro II tandem quadrupole mass spectrometer coupled to a Shimadzu LC. An R2 reverse-phase LC column was used for separation. The mass spectrometer was run in electrospray-ionization mode (ESI) at a cone voltage of 55 V, with a source block temperature of 100 °C and a desolvation temperature of 350 °C. The molecular weight of the ^{15}N-Phe-labeled and unlabeled $P450_{eryF}$ was determined to be 44 968 and 44 985, respectively. The purity of $P450_{eryF}$ was determined by SDS−PAGE analysis to be >95%. The concentration and purity of P450 was determined using UV/vis spectroscopy of the CO reduced, reduced with >99% in the P450 form.

Absorbance Spectroscopy. The absorbance experiments with CYP3A4 were performed using a Cary 3E absorbance spectrophotometer (Varian Scientific Instruments, Inc., Lake Forest, CA) or an Olis Modernized Aminco DW-2 (Olis, Inc., Bogart, GA) as previously described (*21*−*23*). All samples contained 100 mM phosphate (pH 7.4) and were performed at 25 °C.

Absorbance spectra were deconvoluted into their low- and high-spin components and the broad δ band using the multiple-peak fitting package of Igor Pro 5.0 (Wavemetrics, Inc., Lake Oswego, OR) in a similar fashion as described for $P450_{CAM}$ and CYP3A4 (*18*, *24*). The relative areas under these peaks were calculated and compared to the low-spin reference spectra to estimate percentages of low and high spin.

If the ligands of $P450_{eryF}$ have a strong effect on the extinction coefficients of the low-spin Soret band, which is

[2] The K_S derived from the Hill equation is not a true dissociation constant. Therefore, the abbreviation, K_S (Hill), will be used to differentiate between Hill-equation-derived K_S values and K_S values determined by model fitting.

the case for $P450_{eryF}$ in the presence of 9-AP, then the method described above will not work. However, the low- and high-spin Soret of the ligand-bound $P450_{eryF}$ can be compared to the low- and high-spin Soret peaks of $P450_{eryF}$ with known percentages of low and high spin (e.g., $P450_{eryF}$ without ligands). Therefore, the areas of Soret peaks of $P450_{eryF}$ with known percentages of high and low spin were compared with the area of the corresponding peaks in $P450_{eryF}$ with saturating ligand, using the relationship between the areas under these peaks and their spin-state equilibrium (K_{SPIN}). K_{SPIN} is related to the concentration of low spin and high spin by the following relationship, where HS = high spin, LS = low spin:

$$K_{SPIN} = \frac{[HS]}{[LS]} = \frac{\%\ HS}{\%\ LS} \quad (1)$$

K_{SPIN} is related to the areas (A_{HS} = area under high-spin Soret band; A_{LS} = area under low-spin Soret band; C = constant) under the Soret bands by the following:

$$K_{SPIN} \propto \frac{A_{HS}}{A_{LS}} = C\frac{A_{HS}}{A_{LS}} \quad (2)$$

Using the above relationship, C', K_{SPIN}', A_{HS}', and A_{LS}' from the $P450_{eryF}$ with unknown percentages of low and high spin, denoted by a prime (i.e., ′), can be compared to C, K_{SPIN}, A_{HS}, and A_{LS} of the $P450_{eryF}$ with known percentages of low and high spin

$$\frac{\dfrac{C'A_{HS}'}{A_{LS}'}}{K_{SPIN}'} = \frac{\dfrac{CA_{HS}}{A_{LS}}}{K_{SPIN}} \quad (3)$$

Let us assume that the effect of the ligand is the same affect on the extinction coefficients of the low- and high-spin Soret bands or $C \approx C'$, then

$$K_{SPIN}' = K_{SPIN}\frac{A_{HS}'}{A_{LS}'}\cdot\frac{A_{LS}}{A_{HS}} \quad (4)$$

From this, the high spin and low spin can be calculated

$$K_{SPIN}' = \frac{\%\ HS}{\%\ LS} = \frac{\%\ HS}{100 - \%\ HS} = \frac{100 - \%\ LS}{\%\ LS} \quad (5)$$

This method allows one to calculate the % low spin and % high spin without using a low-spin control. However, a standard sample with known % low spin and % high spin must be used.

NMR Spectroscopy. All NMR spectra were obtained at 25 °C on a Varian Unity Inova 500 MHz NMR spectrometer, equipped with a Varian $^1H\{^{13}C/^{15}N\}$ triple resonance (TR)/pulse-field-gradient (PFG) probe (Varian, Inc., Palo Alto, CA). All NMR data sets were processed on a Silicon Graphics O2 workstation (Silicon Graphics, Inc., Mountain View, CA) using the NMRPipe System Software (*25*) or on a personal computer with MestreC version 3.992 (MestreC, A Coruña, Spain). Two-dimensional-$\{^1H,^{15}N\}$-heteronuclear single-quantum coherence (HSQC) NMR spectra with water suppression by gradient selection were carried out at various concentrations of 9-AP and TST in 50 mM phosphate (pH 7.4, 25 °C) in 10% D_2O. These spectra were obtained at a ^1H and ^{15}N radio frequency power of 57 dB (i.e., ∼17 W) and 56 dB, respectively, with ^{15}N decoupling during acquisition at a decoupling power of 42 dB. Further details of the NMR experiment can be found in ref *26*.

Simulations of the NMR and Absorbance Data. The changes in the absorbance spectra were fit, using GEPASI (*27*−*29*). The fits were based on the sequential-ordered binding model, the simplest model to fit the data, which has already been demonstrated for CYP3A4 (*18*, *19*)

$$P450 \overset{K_S}{\rightleftharpoons} P450{\cdot}L \overset{\alpha K_S}{\rightleftharpoons} P450{\cdot}L{\cdot}L$$

$$P450 \underset{k_{-1}}{\overset{k_1}{\rightleftharpoons}} P450{\cdot}L \underset{k_{-2}}{\overset{k_2}{\rightleftharpoons}} P450{\cdot}L{\cdot}L$$

$$K_S = \frac{k_{-1}}{k_1} \quad (6)$$

$$\alpha K_S = \frac{k_{-2}}{k_2} \quad (7)$$

The actual concentrations of [P450], [P450·L], [P450·L·L], and [L] were determined using the rate equations below, rather than equilibrium equations, such as the Adair−Pauling equation. The equilibrium equations cannot be used to accurately determine the K_S values, when the [P450] concentration is high with respect to the K_S. The [P450] was high with respect to K_S for the absorbance experiment with 9AP and the NMR experiments. Therefore, the steady-state solutions using the rate equations were used to determine the K_S values, which allows for an accurate measurement of the K_S values regardless of the [P450]. Below are the rate equations that were used to determine the steady-state concentrations of [P450], [P450·L], [P450·L·L], and [L], on the basis of the sequential-ordered binding mechanism

$$\frac{\partial[P450{\cdot}L]}{\partial t} k_1[P450][L] + k_{-2}[P450{\cdot}L{\cdot}L] - k_{-1}[P450{\cdot}L] - k_{-2}[P450{\cdot}L][L] \quad (8)$$

$$\frac{\partial[P450{\cdot}L{\cdot}L]}{\partial t} = k_2[P450{\cdot}L{\cdot}L] - k_{-2}[P450{\cdot}L{\cdot}L] \quad (9)$$

$$\frac{\partial[L]}{\partial t} = k_{-1}[P450{\cdot}L] + k_{-2}[P450{\cdot}L{\cdot}L] - k_1[P450][L] - k_2[P450{\cdot}L][L] \quad (10)$$

The effect on the spin state of the first ligand versus the second ligand on $P450_{eryF}$ is not expected to be identical. Therefore, the changes in the absorbance spectra are likely to have this relationship

$$A = \sigma_1[CYP{\cdot}L] + \sigma_2[CYP{\cdot}L{\cdot}L] \quad (11)$$

where A = amplitude of the absorbance change, σ_1 = spin coefficient of [CYP·L], σ_2 = spin coefficient of [CYP·L·L].

The spin coefficients are related to the fractional change in the spin state. To be consistent, a positive spin coefficient ($\sigma > 0$) represents a shift to the high-spin state, while a negative spin coefficient ($\sigma < 0$) represents a shift to the

low-spin state. The fractional change of the spin state can be determined with

$$f_{s_1} = \frac{\sigma_1}{|\sigma_1| + |\sigma_2|} \quad (12)$$

$$f_{s_2} = \frac{\sigma_2}{|\sigma_1| + |\sigma_2|} \quad (13)$$

where f_{s_1} = fractional change in the spin state by the first ligand and f_{s_2} = fractional change in the spin state by the second ligand.

The steady-state concentrations determined from the rate equations as described in refs *27*−*29* were inputed into eq 11. The values determined by simulations of the absorbance spectra, using eq 11, were also fit to the NMR titration data as a cross-check for consistency between the two methods used to probe for binding.

RESULTS

UV/Vis-Monitored Titration of P450$_{eryF}$ with Ligands, 9-AP, and TST. Difference spectroscopy of the UV/vis Soret bands (∼390−420 nm) of P450's in the presence and absence of ligands has been used previously to determine the effect of the ligand on the local heme environment of P450 (*18*, *30*). A difference spectrum showing increases at >420 nm and decreases at <390 nm reflects a ligand-induced shift of the P450 heme to the low-spin state, which is often characterized by the direct association of a nitrogen or oxygen of the ligand to the heme. On the other hand, a difference spectrum showing decreases at >420 nm and increases at <390 nm reflects a ligand-induced shift of the P450 heme to the high-spin state, which is associated with the ligand's displacement of the water that is bound to the heme.

Figure 1 shows 9-AP-induced changes on UV/vis difference spectra of P450$_{eryF}$. Figure 1A (inset) shows the absorbance difference of the Soret region observed between P450$_{eryF}$ at various concentrations of 9-AP minus P450$_{eryF}$ without 9-AP ([P450$_{eryF}$ + 9-AP] − [P450$_{eryF}$]). There is an absorbance decrease at approximately 414 nm and an absorbance increase at 434 nm, consistent with the ligand shifting the P450$_{eryF}$ heme into the low-spin state (*13*). The difference in the amplitudes between 434 and 414 nm as a function of the 9-AP concentration is shown in Figure 1B with the fit of the sequential ordered binding model as a solid line. The Hill plot analysis of Figure 1A is shown in Figure 1B. The K_S (Hill) = 4 ± 0.7 μM and the n = 1.4 ± 0.2 were extracted from this plot and agree with previous results [K_S (Hill) = 7.8 μM, n = 1.62 (*13*)].

Figure 2 shows TST-induced changes on UV/vis difference spectra of P450$_{eryF}$. The absorbance difference plotted in Figure 2A (inset) shows an absorbance increase at 388 nm and an absorbance decrease at 420 nm, consistent with a TST-induced shift of the P450 heme to the high-spin state (*17*). The difference between these wavelengths is shown in Figure 2A (*17*). A fit of the simulation based on the sequential-ordered binding model is shown in Figure 2B (—), and the Hill plot analysis is shown in Figure 2B.

The ligand-induced spin-state shift was found to have apparent negative cooperativity (n = 0.89 ± 0.13) by the Hill analysis, and the binding was considerably weaker than for 9-AP [K_S (Hill) = 230 ± 44.5 μM]. These results are in qualitative agreement with previous binding results [K_S (Hill) = 410 μM] (*17*).

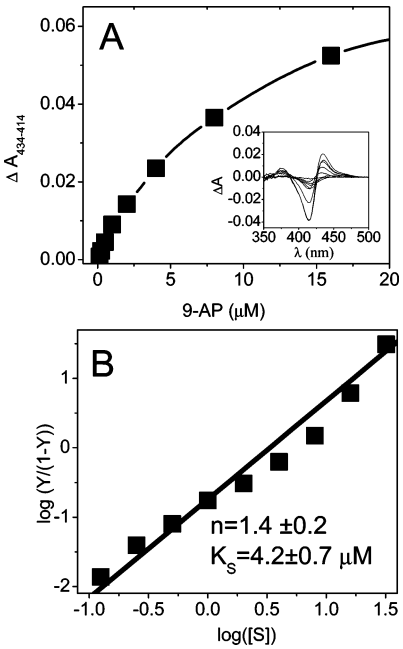

FIGURE 1: Equilibrium binding titration of P450$_{eryF}$ with 9-AP by UV/vis difference absorbance spectroscopy. A (inset) shows the individual absorbance difference curves at a range of 9-AP concentrations in micromolars. A shows the absorbance difference of 434 − 414 nm of P450$_{eryF}$ at a range of 9-AP concentrations in micromolars. B is a Hill plot analysis of B. The [P450] was approximately 1 μM for these experiments.

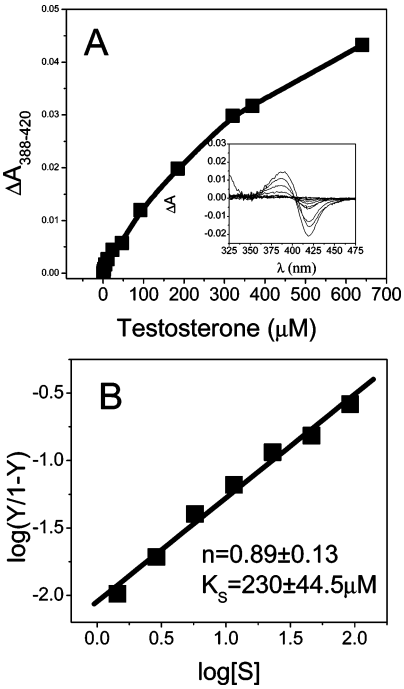

FIGURE 2: Equilibrium binding titration of P450$_{eryF}$ with TST by UV/vis difference absorbance spectroscopy. A shows the individual absorbance difference curves at a range of TST concentrations in micromolars. B shows the absorbance difference of 388 − 420 nm of P450$_{eryF}$ at a range of TST concentrations in micromolars. C is a Hill plot analysis of B. The [P450] was approximately 1 μM for these experiments.

The Hill plot analysis is useful for providing a qualitative view of affinity and cooperativity yet provides little information about the individual binding events. However, simulating the UV/vis difference of P450's to models that reasonably represent the binding can provide important insights into binding and allostery. The dissociation constants (K_S and αK_S) determined from a simulation can provide the thermodynamic information about the predominant binding steps and the coupling free energy between these steps, which is itself a useful measure of cooperativity (see the Discussion).

A simulation of data in Figure 1B based on a sequential-ordered binding mechanism (see the Materials and Methods) is shown as a solid line in Figure 1B. From the simulation, the K_S and αK_S were determined to be 13.48 ± 1.45 mM and 2.01 ± 0.99 μM. The spin coefficients were determined to be -0.0598 ± 0.00359 and -0.0595 ± 0.00573 for σ_1 and σ_2, respectively, because 9-AP is a low-spin ligand (recall that $\sigma < 0$ corresponds to a low-spin transition, as explained in the Materials and Methods). The fractional contribution of each bound state, P450·L and P450·L·L, toward shifting the heme to the low-spin state was about $50 \pm \sim 8\%$ (i.e., 50% per binding event).

Simulations of the TST-induced absorbance changes in Figure 2B of $P450_{eryF}$ show the $K_S = 286 \pm 19.7$ μM and $\alpha K_S = 795 \pm 41.2$ μM for the first and second binding, respectively. The spin coefficients were $\sigma_1 = 2.5 \times 10^{-4} \pm 1 \times 10^{-5}$ and $\sigma_2 = 1.8 \times 10^{-4} \pm 2 \times 10^{-5}$, giving a fractional change of $f_{s_1} = 57.5 \pm 6.4\%$ and $f_{s_2} = 42.5 \pm 7.6\%$, respectively. Because the "first" ligand elicits an apparent stronger spin-state change on average, it is likely to be bound closer to the heme than the "second" ligand. The simulations and the Hill analysis, however, provide no information of the binding mechanism for the apparent negative cooperativity. The apparent negative cooperativity could be the result of noninteracting (independent) binding sites, where there is a relatively tight and weak binding site, or "classical" negative cooperativity, where one site reduces the binding affinity for the second site. Regardless of the actual binding mechanism, the fact is that the ligand distribution between binding sites at low [TST] would behave functionally as negative cooperativity in both cases. In other words, TST would preferentially bind to the relatively tight binding site over the weak binding site at low [TST].

Peak Fitting Analysis of UV/Vis Absorbance Peaks of $P450_{eryF}$ in the Presence of TST and 9-AP. The absolute UV/vis Soret (325−500 nm) region of P450's can be deconvoluted into a δ band, a low-spin Soret, and high-spin Soret bands. The low-spin and high-spin Soret bands have been assigned to the low- and high-spin states of the P450 heme, respectively. On the other hand, the δ band has not been assigned an obvious function in the literature. With appropriate controls, peak fitting can be used to determine the concentration of low and high spin in the sample as previously described (*18*). Knowing these relative concentrations is critical for interpreting NMR data because increasing the concentration of high spin can lead to paramagnetic broadening and shifting (*1*, *31*), which contribute to (and thus be misinterpreted as) the diamagnetic exchange broadening and chemical shifting caused by ligand binding to the P450. The % low spin and % high spin calculated from the Soret bands of $P450_{eryF}$ with and without saturating ligands are shown in Table 1.

Table 1: % Low Spin and High Spin in $P450_{eryF}$ with TST and 9-AP Compared with the Quantities of % Low Spin and High Spin in CYP3A4 with TST

	% low spin	% high spin	|Δ% spin state[a]|
$P450_{eryF}$ (unbound)	93	7	
$P450_{eryF}$ + TST	75	25	18%
$P450_{eryF}$ + 9-AP	97	3	4%
CYP3A4 (unbound)	83[b]	17[b]	
CYP3A4 + TST	50[b]	50[b]	33%[b]

[a] Δ% spin state was determined by taking the absolute value of the difference between ligand-bound P450 or CYP and ligand-free P450 or CYP. [b] Values taken from ref *18*.

Figure 3A shows the low- and high-spin Soret bands in the presence of 22 mM aniline, which will be assumed to be ~100% low spin. The δ band and low-spin Soret bands were found at 360 and 423 nm, respectively.

Figure 3B shows the low- and high-spin Soret bands in the absence of ligands. Deconvoluting the spectrum reveals that it is comprised of the three expected components: the δ band, the low-spin band, and the high-spin Soret bands. These peaks were found at 360, 394, and 418 nm, respectively. Assuming that the aniline sample (in Figure 3A) represents ~100% low spin, we determined the low-spin concentration in these samples to be ~93% (and therefore, 100% − 93% = 7% high spin). We compare this result to the low-spin concentration determined for CYP3A4 in the absence of ligands (% low spin = 83%) (*18*, *32*).

Figure 3C shows the affect of close to saturating TST (640 μM) on the absolute absorbance spectrum of $P450_{eryF}$. Deconvolution of the spectrum revealed the same three peaks at 360, 393, and 418 nm but with a decrease in the low-spin Soret band and an increase in the high-spin Soret band. Using $P450_{eryF}$ with aniline as a low-spin control, $P450_{eryF}$ with TST was found to have 75% low spin and therefore 25% high spin. A high-spin concentration of 7% in the absence of TST versus 25% in the presence of TST means that TST induces a modest 18% increase in high spin. This is a much smaller increase than was observed for CYP3A4 (17% high spin in the absence of TST versus 50% high spin in the presence of TST = 33% increase in high spin) (*18*).

Figure 3D shows the affect of saturating 9-AP on the absolute absorbance spectrum of $P450_{eryF}$ with a δ band, high-spin Soret, and low-spin Soret at 385, 402, and 423 nm. There is a 50% decrease in area of the low-spin Soret peak, which would normally indicate a decrease in the low-spin concentration. If there were a decrease in the low-spin concentration, a corresponding increase in the high-spin concentration would result. Instead, there is a 75% decrease in the high-spin Soret band, a counterintuitive result. However, because the decrease in the area of the high-spin Soret peak (i.e., 75%) is greater than the decrease in the area of the low-spin Soret peak (i.e., 50%), the relative change in area between low spin and high spin suggests a shift to low spin, which is in line with expectations. Because of these effects on the $P450_{eryF}$ Soret bands by 9-AP, the relative concentration of low spin in the $P450_{eryF}$ with 9-AP cannot be directly determined from the low-spin Soret of $P450_{eryF}$ with saturating aniline as is possible with $P450_{eryF}$ with TST or without ligands. Therefore, the concentration of low spin and high spin in $P450_{eryF}$ with 9-AP was determined by comparing the areas of the low- and high-spin Soret peaks

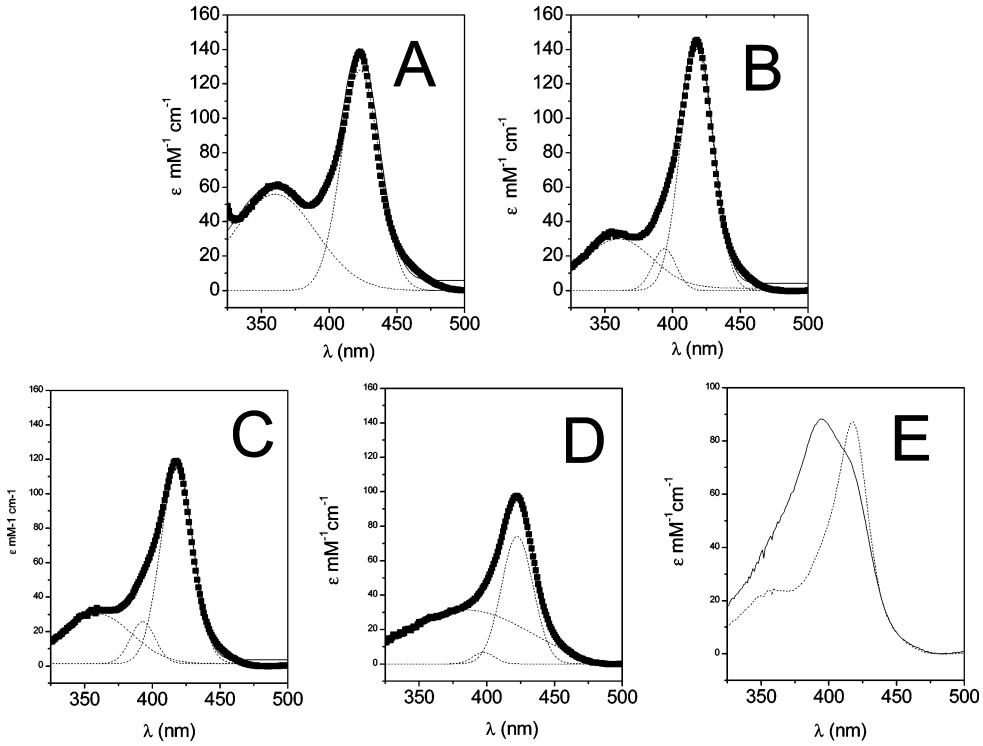

FIGURE 3: Change in the high-spin concentration of P450$_{eryF}$ determined by absorbance spectroscopy. Curve fitting of the absorbance spectra of P450$_{eryF}$ with (A) aniline ($R = 0.99$), (B) no ligands ($R = 0.98$), (C) close to saturating TST (i.e., 640 μM) ($R = 0.97$), and (D) saturating 32 μM 9-AP ($R = 0.99$) was used to determine the relative change in % low spin and high spin. The experimental data is shown as ■, and the fit is shown as —. The Gaussian curves used to fit the experimental data are shown as ···. E shows a comparison of P450$_{eryF}$ (—) and CYP3A4 (···) at near saturating TST.

of P450$_{eryF}$ with 9-AP to P450$_{eryF}$ without ligands (see the Materials and Methods, eqs 1−7). From this analysis, P450$_{eryF}$ with 9-AP was found to have 97% low spin and 3% high spin, which is a very small 4% change in the spin state.

Electron paramagnetic resonance (EPR) spectroscopy of P450$_{eryF}$ was performed at 5 K to determine if the analysis above was correct, i.e., that the heme of P450$_{eryF}$ was indeed shifted to the low-spin state upon binding of 9-AP. As expected, no EPR high-spin signal from P450$_{eryF}$ in the presence of 9-AP was observed at 5 K (data not shown). These EPR results support the UV/vis data and are consistent with 9-AP shifting the P450$_{eryF}$ to >93% low spin.

Further evidence of the small spin state changes in the presence of these ligands is demonstrated in Figure 3E. Figure 3E compares the absolute absorbance of CYP3A4 (—) and P450$_{eryF}$ (···) normalized to the CYP3A4 high-spin Soret band in the presence of close to saturating TST. The amplitude of the absorbance at ~390 nm shows that the concentration of high spin is clearly higher for CYP3A4 than for P450$_{eryF}$ at similar TST concentrations.

2D-{^{1}H,^{15}N}-HSQC-Monitored Titration of P450$_{eryF}$ with Ligand 9-AP. P450$_{eryF}$ contains 17 phenylalanine residues, 8 of which are in the active-site pocket (F72, F78, F86, F109, F167, F243, F344, and F350 in Scheme 1). Their proximities to bound ligand and/or heme suggest that these Phe's participate in the formation of the P450$_{eryF}$−ligand complex, either directly via ring stacking to the aromatic portions of the bound ligand or indirectly via conformational rearrangements in the active-site pocket that accompany binding (*5*, *33*, *34*). Interestingly, site-directed mutagenesis of P450$_{eryF}$ to P450$_{eryF}$ (F78W) decreases the degree of cooperative

Scheme 1: Active Site of P450$_{eryF}$, Showing Important Active-Site Phe's and the Phe's from Related Structures[a]

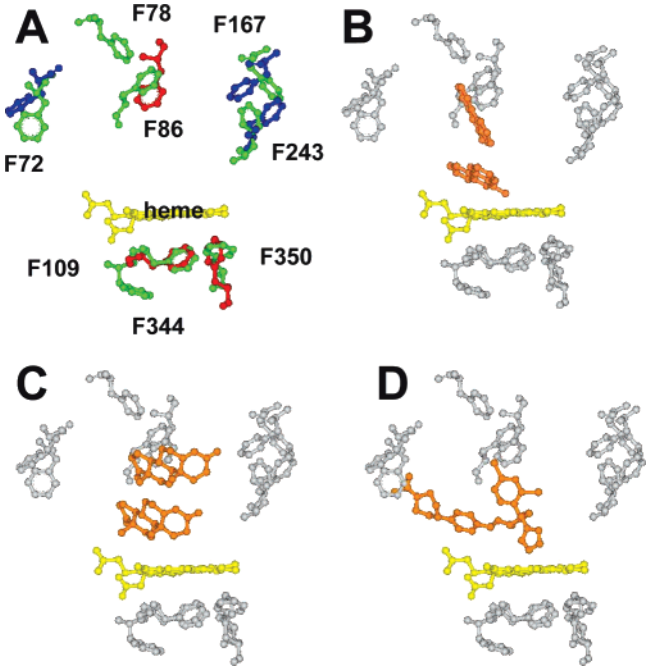

[a] (A) Important Phe's from the 9-AP-bound P450$_{eryF}$ (green) (*5*), significantly shifted Phe's from the ketoconazole-bound P450$_{eryF}$ (blue) (*33*), Phe's from the CYP3A4 structure (red) (*44*, *45*) that overlap with the active-site Phe's of P450$_{eryF}$. Also, shown is the heme (yellow). (B) 9-AP (orange) bound to P450$_{eryF}$ with the heme (yellow) and the active-site Phe's (gray). (C) Androstenedione (orange) bound to P450$_{eryF}$ with the heme (yellow) and the active-site Phe's (gray). (D) Ketokonazole (orange) bound P450$_{eryF}$ with the heme (yellow) and the active-site Phe's (gray).

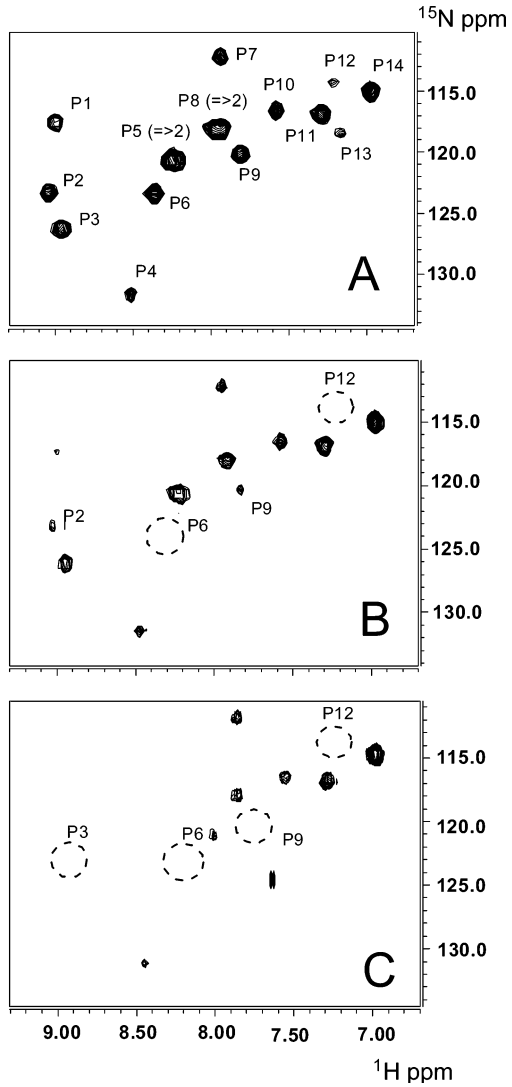

FIGURE 4: Equilibrium binding titration of P450$_{eryF}$ with 9-AP by 2D NMR spectroscopy. ^{1}H 2D-{^{15}N,^{1}H}-HSQC correlation spectra (500 MHz) obtained at 298 K (25 °C) of 200 μM P450$_{eryF}$ (A) in the absence of a ligand and after the addition of about 1 (B) and 2 (C) molar equiv of 9-AP. All peaks are labeled in A. The positions of peaks P2, P6, P9, and P12 are marked in B and C.

behavior exhibited by this enzyme, supporting a possible participation of F78 in the binding of the second 9-AP ligand to P450$_{eryF}$ (*14*).

On the basis of the studies outlined above, we uniformly incorporated ^{15}N-labeled Phe as a probe of changes in the chemical environment and dynamics of the P450$_{eryF}$ active-site pocket that accompany binding of the ligand. The selective labeling and detection of only ^{15}N-Phe residues in the 2D-{^{1}H,^{15}N}-HSQC spectrum of [^{15}N-Phe] P450$_{eryF}$ reduces the spectral complexity of the NMR data and allows a simplified mapping of the binding events.

The HSQC spectrum of the free oxidized form of [^{15}N-Phe] P450$_{eryF}$ is shown in Figure 4A. The ^{15}N-Phe amide resonances appear well-dispersed in both dimensions, indicating that P450$_{eryF}$ remains properly folded and active under the NMR working conditions. The spectrum clearly displays 14 resonances (labeled P1−P14 in the figure). The peaks labeled P5 and P8 are composed of >1 overlapping peaks. Therefore, most if not all of the 17 phenylalanines in the P450$_{eryF}$ protein are accounted for as separate peaks in the

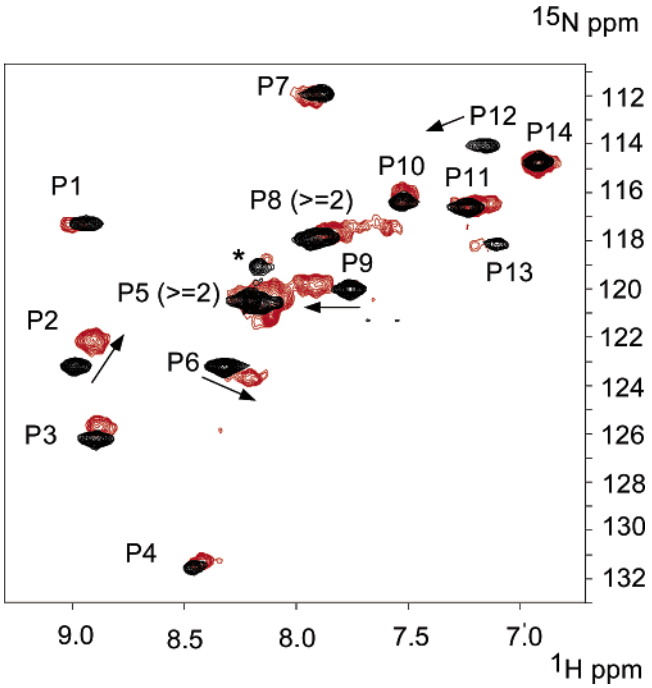

FIGURE 5: Equilibrium binding titration of P450$_{eryF}$ with TST by 2D NMR spectroscopy. ^{1}H 2D-{^{15}N,^{1}H}-HSQC correlation spectra (500 MHz) obtained at 298 K of 283 μM P450$_{eryF}$ in the absence of a ligand (black) and after the addition of about 6 molar equiv (1.7 mM) of TST (red). Arrows denote the chemical shifts seen with peaks P2, P6, P9, and P12. Peak P12 is absent at TST concentrations greater than 4.4 molar equiv (1.2 mM).

HSQC spectrum, although not all of these 17 Phe's manifest equal resonance intensity. The decreased resonance intensities of P12 and P13, for example, may result from conformational averaging in the protein, paramagnetic broadening of the one unpaired electron associated with the low-spin state, or amide exhange with the bulk water. Candidates for paramagnetically broadened resonances include F109, F344, and F350, situated closest to the heme (Scheme 1).

Parts B and C of Figure 4 show the 2D-{^{1}H-^{15}N}-HSQC-monitored titrations of [^{15}N-Phe] P450$_{eryF}$ after ~1 and ~2 molar equiv of the 9-AP, respectively. The addition ~1 equiv of 9-AP (Figure 4B) does not lead to shifting in the positions of the resonances but, instead, to significant losses in the resonance intensity, a function of line broadening. The peaks most affected, P2, P6, P9, and P12, lose almost all of their intensity at 2 equiv 9-AP. Table S1 in the Supporting Information lists the intensities for each peak in the titration that were measured from the peak height.

2D-{^{1}H,^{15}N}-HSQC-Monitored Titration of P450$_{eryF}$ with Ligand TST. Two-dimensional-{^{1}H,^{15}N}-HSQC-monitored titrations of [^{15}N-Phe] P450$_{eryF}$ with TST were also performed. Figure 5 plots the HSQC spectrum of the free oxidized form of [^{15}N-Phe]P450$_{eryF}$ (in black contours) overlayed with the HSQC spectrum of the oxidized [^{15}N-Phe]P450$_{eryF}$ in the presence of 12.0 molar equiv TST (TST/P450$_{eryF}$ = 12.0) (in red contours). The spectrum clearly displays the 14 resonances (labeled P1−P14 in the figure). Also clearly discernible is the contribution of the two overlapping Phe amide resonances to peaks P5 and P8. These overlapped resonances shift independently of each other in the presence of TST, leading to a "double-lobe" appearance in the bound spectrum.

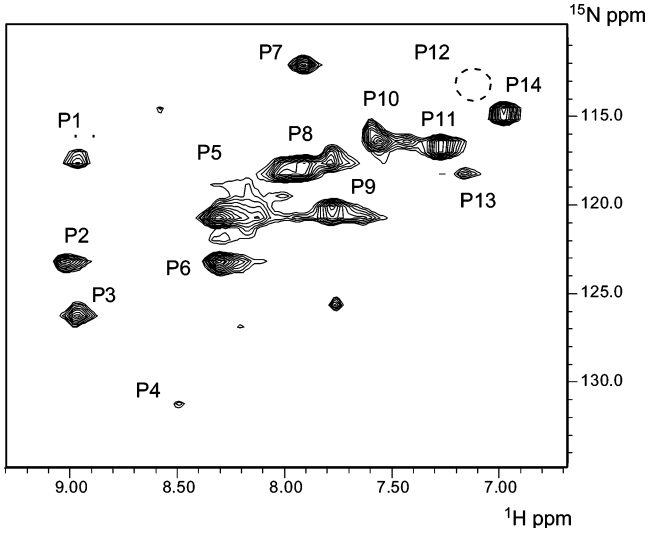

FIGURE 6: Two-dimensional-{^{15}N,^{1}H}-HSQC correlation spectra of the P450$_{eryF}$ F86Y mutant at 298 K. The spectrum shows all of the peaks, except P12, which is shown by a dashed circle.

P5, P8, and P11 exhibit complex spectral behavior by decomposing into smaller peaks. An expanded region of the HSQC spectrum of Figure 5 is presented in the Supporting Information as Figure S1 to illustrate the complicated spectral behavior of P5. P5 breaks into multiple components at TST/P450$_{eryF}$ > 1.0, while P6 remains a single peak throughout the titration. P5 continues to disperse to 12 equiv of TST with roughly 6 components. The striking feature of the dispersal is that the total number of peaks resolved including, P5, P8, and P11, are greater than the total number of Phe's in P450$_{eryF}$, implying that there are different bound/conformational states of TST (see the Discussion). An anomalous peak was found in the HSQC spectrum denoted by an asterisk, which was insensitive to TST. Table S2 in the Supporting Information lists the ^{1}H and ^{15}N chemical shifts for each peak in the titration.

Assignment of F86Y. Only one Phe mutant was found to be amenable to NMR analysis, F86Y. F86Y binds 9-AP (K_S = 5 μM versus K_S = 4 μM for WT; data not shown), suggesting a properly folded active site. Unsurprisingly, the cooperativity with 9-AP is significantly decreased for F86Y, with n = 1.1 for the mutant versus n = 1.4 for the wild type (data not shown).

Figure 6 is the 2D-{^{15}N,^{1}H}-HSQC spectrum of the ^{15}N-Phe-labeled F86Y P450$_{eryF}$ mutant. All peaks are at their WT chemical shifts, barring some subtle spectral differences related to folding and solubility issues. The exception is P12 (absent in the dashed circle in Figure 8). The continued absence of this peak in different fresh NMR samples of ^{15}N-Phe-labeled F86Y, coupled with the persistence of all other peaks in an otherwise "WT-like" spectrum, allows P12 to be assigned to F86. The fact that P12, a peak significantly broadened and shifted in the 9-AP and TST titrations, likely corresponds to an active-site phenylalanine involved in ligand binding, suggests that the ligand-induced NMR perturbations observed in the HSQC spectra are localized to the active site and are not global in nature.

Analysis of "Binding Niches" for 9-AP versus TST. Figure 7 presents plots of the spectral changes (i.e., broadening for 9-AP and shifting for TST) observed for P450$_{eryF}$ in the presence of 9-AP and TST. Figure 7A plots changes in peak intensities ($\delta I = I^{free} - I^{bound}$ in arbitrary units, where I^{free} = the peak intensity at 9-AP/P450$_{eryF}$ = 0, and I^{bound} = the peak intensity at 9-AP/P450$_{eryF}$ ~ 2) measured in the

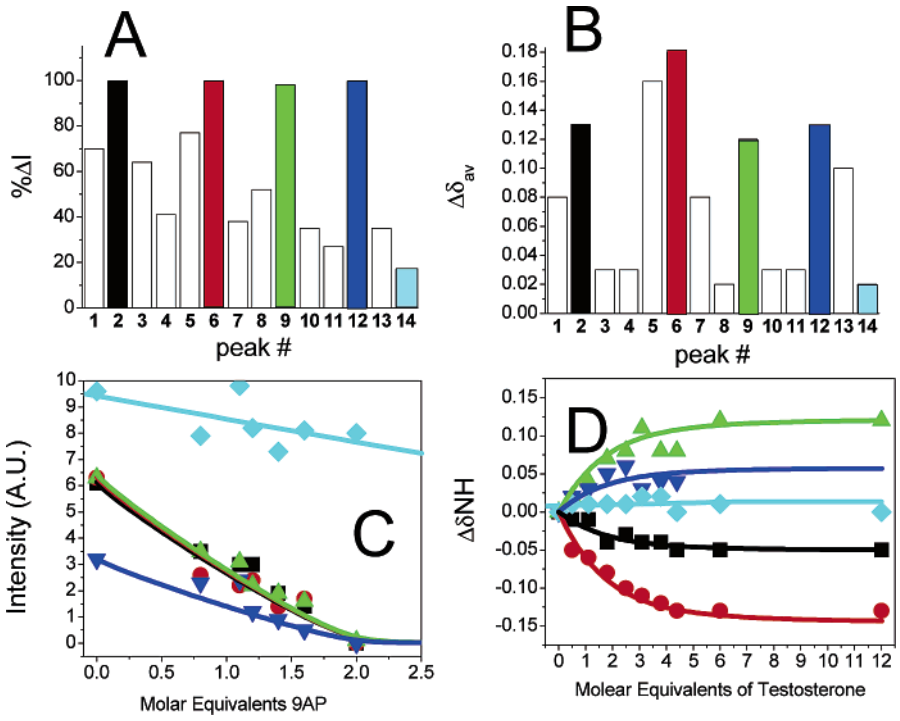

FIGURE 7: Quantitative changes in the P450$_{eryF}$ spectra in the presence of 9-AP (A and C) and TST (B and D). (A) Absolute value change of the peak intensity of P450$_{eryF}$ versus the peak number in the presence of 9-AP. (B) Weighted average $\Delta\delta_{av}$ observed for P450$_{eryF}$ in the presence of TST. $\Delta\delta_{av} = [\Delta\delta_{NH}^2 + (\Delta\delta^{15}_{N}/5)^2]^{1/2}$, where $\Delta\delta = \delta_{free} - \delta_{bound}$ and δ_{free} is the chemical shift at TST/P450$_{eryF}$ = 0, and δ_{bound} is the chemical shift at TST/P450$_{eryF}$ = 12.0 (see refs *35* and *36*). (C) Absolute intensity of 9-AP peaks with respect to molar equivalents of 9-AP. (D) $\Delta\delta_{NH}$ with respect to molar equivalents of TST, where $\Delta\delta_{NH}$ represents $\delta_{NH,free} - \delta_{NH,bound}$. The peaks P2, P6, P9, P12, and P14 are color-coded.

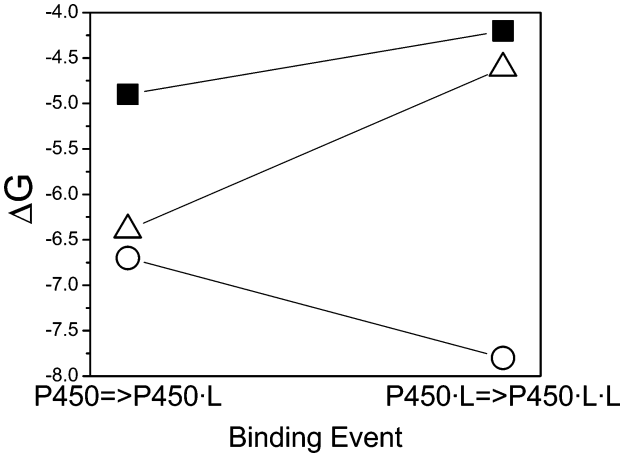

FIGURE 8: Plot of free energy (ΔG) as a function of the binding event between P450 → P450·L and P450·L → P450·L·L. The free energies of binding of the first and second TST (■) and 9-AP (○) to $P450_{eryF}$. Also shown are the free energies of binding the first and second TST in CYP3A4 (△).

HSQC-monitored titration of [^{15}N-Phe] $P450_{eryF}$ with 9-AP. Figure 7B plots the weighted average of the chemical shift $[\Delta\delta_{av} = [\Delta\delta_{NH}^2 + (\Delta\delta^{15}_{N}/5)^2]^{1/2}$, where $\Delta\delta = \delta^{free} - \delta^{bound}$, δ^{free} = the chemical shift at TST/$P450_{eryF}$ = 0, and δ^{bound} = the chemical shift at TST/$P450_{eryF}$ = 12.0 (see refs *35* and *36*)] measured in the HSQC-monitored titration of [^{15}N-Phe]$P450_{eryF}$ with TST. With the exception of P5, which is comprised of two overlapping resonances and therefore subject to some error in the intensity measurement, the binding of 9-AP and TST to $P450_{eryF}$ leads to significant perturbations of the same 4 Phe's, those corresponding to P2, P6, P9, and P12. This remarkably similar collection of "most perturbed peaks" suggests that 9-AP and TST share similar "binding niches". In other words, 9AP and TST that are bound in the active site interact with the same Phe's.

Simulations of the spectral changes observed for $P450_{eryF}$ in the presence of 9-AP and TST were performed next, using the concentrations of $P450_{eryF}$ used in the NMR experiments (i.e., 200 and 280 μM) and the parameters (i.e., K_S, αK_S, σ_1, and σ_2) determined from the UV/vis analysis (Figures 1 and 2).

For 9-AP, the amplitudes of P2, P6, P9, and P12 decrease asymptotically to 0 intensity at 2 equiv 9-AP in a manner that is consistent with intermediate exchange with respect to the chemical shift. The asymptotic behavior is consistent with the high protein concentration used in these experiments (i.e., [$P450_{eryF}$] = 200 μM) (for a review, see ref *37*). The simulation of 9-AP binding was normalized to the data points (—) and shows a reasonable fit, suggesting that the exchange of 9-AP is in a range of intermediate exchange, where the relationship between the enzyme−substrate complex and resonant peak amplitude is relatively linear (*38*−*40*).

For TST, the shifting observed for P2, P6, P9, and P12, which is characteristic of fast exchange with respect to the chemical shift, also appears to fit well to the simulations, which would be expected for this exchange regime (*38*−*40*). In addition, the appearance of peak dispersal from our analysis of P5 (Figure S1 in the Supporting Information) at greater than 1 equiv TST suggest binding of multiple TST molecules. The peaks continue to shift up to 12.0 molar equiv TST, where the $P450_{eryF}$ binding site is primarily saturated, although precipitation was observed at lower concentrations.[3]

DISCUSSION

Several ligands are known to exhibit homotropic and heterotropic cooperativity in binding to $P450_{eryF}$ (*5*, *13*, *17*), and thus, $P450_{eryF}$ has been deemed a useful model for cooperativity in P450's and CYP's. Although a couple of X-ray crystal structures of $P450_{eryF}$ have been solved with ligands that exhibit homotropic cooperativity (*5*), little is known about the dynamics and energetics of the ligands that exhibit homotropic cooperativity.

Dynamics of 9-AP and TST Binding to $P450_{eryF}$. Spectral perturbations observed in the 2D-{^{1}H,^{15}N}-HSQC-monitored titration of [^{15}N-Phe]$P450_{eryF}$ with 9-AP showed decreases in the resonance intensity, as a function of the 9-AP concentration. This loss of intensity is unlikely as a result of paramagnetic broadening effects, associated with the unpaired electron(s) of the heme, because there is only a 4% increase in low spin in the presence of 9-AP (see the Results). Paramagnetic broadening of the peaks would be more expected for a shift to the high-spin state, where the total number of unpaired electrons increases.[4] Furthermore, F86 (assigned to P12 on the basis of mutagenesis), which lies 16 Å from the heme Fe^{3+}, would not be expected to be paramagnetically broadened but, nevertheless, exhibits strong line broadening in the presence of 9-AP. Together, these results infer that the peak broading observed in the 2D-{^{1}H,^{15}N }-HSQC-monitored titration of [^{15}N-Phe]$P450_{eryF}$ with 9-AP is primarily due to intermediate chemical exchange on the chemical-shift time scale ($\Delta\delta \sim k_{ex}$, where $\Delta\delta$ = the chemical-shift difference between ligand-bound and ligand-free states and k_{ex} = the chemical-exchange rate) (*41*−*43*).

In contrast, the spectral perturbations observed in the 2D-{^{1}H,^{15}N}-HSQC-monitored titration of [^{15}N-Phe]$P450_{eryF}$ with TST showed shifting in the position of the resonances as a function of the TST concentration. The shifting of most of the peaks is consistent with a fast exchange on the chemical-shift time scale ($\Delta\delta \ll k_{ex}$, where $\Delta\delta$ = the chemical-shift difference) (*41*−*43*). However, the complex dispersion observed for P5, P8, and P11 may represent a slow conformational exchange on the NMR time scale (*41*−*43*). The assumption of an intermediate exchange for the 9-AP titration but a fast exchange for most of the peaks in the TST titration is supported by the value of the K_S (Hill) values of the two ligands for $P450_{eryF}$ (K_S = 4−7.8 μM for 9AP versus K_S = 200−410 μM for TST; this study and refs *13* and *17*).

[3] No precipitate was noticeable in the NMR tube until TST/$P450_{eryF}$ > 4. The precipitate is believed to consist of mainly TST because the 2D-HSQC spectra did not show any sign of $P450_{eryF}$ aggregation (as would be indicated by a loss of resonance intensity, uniform line broadening of protein resonances, or the appearance of visible protein aggregates in the bottom of the tube).

[4] The degree of paramagnetic relaxation elicited on nearby nuclei scales to the total number of unpaired electrons associated with the metal center. Fe^{3+} in its high-spin state has five unpaired electrons, whereas Fe^{3+} in its low-spin state has only one unpaired electron. Paramagnetic broadening of NMR resonances is therefore highly pronounced in the HSQC spectra of proteins of high-spin iron centers, as shown in the 2D-{^{1}H,^{15}N}-HSQC of myoglobin (*1*).

Phenylalanines Play an Important Role in 9-AP and TST Binding. Despite the differences in relative affinities between 9-AP and TST, which gave rise to different spectral perturbations (broadening for 9-AP and shifting for TST) and different homotropic cooperative behavior, the collection of resonances most perturbed by the binding of 9-AP versus TST was the same in each titration (P2, P6, P9, and P12).

The X-ray crystal structures of $P450_{eryF}$ with 9-AP, androstenedione, and ketoconazole were compared to elucidate the important Phe's in the $P450_{eryF}$ active site (*5*, *20*, *33*, *34*). Scheme 1 shows the Phe's of $P450_{eryF}/(9\text{-AP})_2$, $P450_{eryF}/(\text{androstenedione})_2$, and $P450_{eryF}$/ketoconazole that were deemed to be in the active site (*5*, *20*, *33*, *34*). While no crystal structures exist for the $P450_{eryF}/(TST)_2$ complex, the structural and chemical similarities between TST and androstenedione suggest that two molecules of TST might bind in a similar mode and interact with the same Phe's as do the molecules of androstenedione. This model of TST binding alludes to a potential mechanism for the apparent negative cooperativity observed in the absorbance titrations. The TST closest to the heme (proximal TST), which binds tightest, forms the binding site for the TST furthest from the heme (distal TST). When the binding site for the distal TST is formed, the proximal TST can "reduce" the binding affinity of the second TST for $P450_{eryF}$. In this case, TST exhibits "classical" homotropic negative cooperativity.

Qualitative inspection of ligand-bound $P450_{eryF}$ structures reveals that 9-AP and androstenedione occupy similar niches within the $P450_{eryF}$ active site, while the bulkier ketoconazole appears to occupy a larger part of the active site, interacting with F72 and causing conformational changes in F167 and F243. 9-AP and androstenedione molecules that are proximal to the heme are closest to F350, F109, and F344, which reside on the opposite side of the heme (*5*). 9-AP and androstenedione molecules that are distal to the heme are close to F78 and F86 (*5*). Because the strongest spectral perturbations would be expected for these Phe's, these are clearly candidates for P2, P6, P9, and P12. Already, P12 has been assigned F86, on the basis of our own mutagenesis studies. The F86 ring stacks along with F78 to 9-AP or androstenedione, which is structurally similar to TST, molecules furthest away from the heme in the crystal structure of the $P450_{eryF}/(\text{androstenedione})_2$ and $P450_{eryF}/(9\text{-AP})_2$ (*5*).

9-AP and TST May Exert Local and Global Conformational Changes in $P450_{eryF}$. The remarkable similarity in the identities of the peaks most perturbed in the NMR titrations of $P450_{eryF}$ (P2, P6, P9, and P12) suggests that 9-AP and TST share a similar "binding niche", i.e., that they come into contact with the same Phe's in the $P450_{eryF}$ active site. While it is tempting to conclude that the most perturbed resonances correspond to active-site Phe's only (and the tentative assignment of P12 to F86 supports this line of thinking), the possibility of global conformational changes affecting Phe's far removed from the active site cannot categorically be ruled out. This is especially true given the large number of shifted peaks observed in the HSQC-monitored titrations of $[^{15}\text{N-Phe}]P450_{eryF}$ with TST (Figure 6). Indeed, practically all peaks in the HSQC spectrum experience some chemical shifting, even if the effect is subtle, indicating that binding of TST to $P450_{eryF}$ exerts subtle global changes to the chemical environments of Phe's far removed from the active site.

Unfortunately, no crystal structure of $P450_{eryF}$ has been solved without a ligand bound. Protein crystals produced in the absence of a ligand were needles of poor diffraction quality (Dr. J. R. Cupp-Vickery, personal communication). This may suggest that the structure is different in the absence of a ligand, because we might expect $P450_{eryF}$ to crystallize well in the absence of a ligand, if the structures were identical. However, a comparison of $P450_{eryF}$ crystal structures with different ligands bound show modest displacements of the active-site Phe's from one ligand to the next and no changes in the backbone or side-chain positions of Phe's removed from the active site. These results suggest that global conformational changes induced by ligand binding, if indeed present, are modest.

TST Adopts Multiple Binding Modes in the $P450_{eryF}$ Active Site. As discussed in the Results, several peaks including P5 exhibit complicated spectral behavior throughout the TST titration, breaking up into multiple components at $TST/P450_{eryF} > 1.0$. This complex spectral behavior suggests that the bound TST molecule(s) are experiencing heterogeneity in the chemical environment on the NMR time scale, caused by the sampling of distinct conformational substates and/or different modes of binding within the $P450_{eryF}$ active site. A comparison of the X-ray crystal structures of the ketoconazole versus DEB-bound $P450_{eryF}$ shows that some of the active-site Phe's are capable of undergoing significant conformational changes to accommodate different ligands (*5*, *33*). These crystal structures then support the existence of distinct conformational substates for the $P450_{eryF}$ active site (*33*). Additionally, the observation of chemical heterogeneity but only for $TST/P450_{eryF} > 1.0$ is supportive of multiple binding modes for the second bound molecule of TST. This second TST likely occupies the same niche as the 9-AP furthest from the heme, because the most perturbed peaks (i.e., P2, P6, P9, and P12) are the same in the 9-AP versus TST titrations. Moreover, different binding modes are consistent with the weak binding of the second TST that was determined through simulation (i.e., $\alpha K_S = 795\ \mu M$).

Thermodynamics of 9-AP and TST Binding to $P450_{eryF}$. The energetics of homotropic cooperativity can be best understood in terms of the free energies (ΔG values) of the individual binding events and the difference in the free energies ($\Delta\Delta G$ values). Calculated ΔG values have been useful previously in delineating the mechanism of TST binding to CYP3A4 (*18*). The $\Delta\Delta G$, which is also known as the coupling free energy, can be used as a measure of cooperativity and reflects the energetic coupling between two binding events. The coupling free energy is superior to *n* values determined from the Hill analysis because the coupling free energy is a value of the magnitude of cooperativity between binding events, while *n* is a fitting parameter that is generally believed to be related to the number of binding sites. For positive cooperative binding, the coupling free energy is negative, and for apparent negative cooperative binding, the coupling free energy is positive.

The calculated ΔG and $\Delta\Delta G$ values are shown in Figure 8 with the ΔG plotted as a function of the binding event. The points indicate the relative binding affinities of the averaged predominate binding mode(s), and the lines indicate that there is a relationship between the two binding events.

Positive cooperativity is represented by a negative slope, where the "second binding" event is lower (more favored) than the "first binding" event. Apparent negative cooperativity is represented by a positive slope, where the "second binding" event is higher (less favored) than the "first binding" event. Therefore, this type of analysis is useful for visualizing the magnitude and relationship between binding events of different ligands.

From the simulations of 9-AP binding to $P450_{eryF}$, the K_S and αK_S were determined to be 13.48 and 2.01 μM, respectively. The ΔG of the first and second binding was -6.7 kcal mol^{-1} [$\Delta G_1 = 1.376$ kcal mol$^{-1} \times \log(13.48\ \mu M)$] and -7.8 kcal mol^{-1} [$\Delta G_1 = 1.376$ kcal mol$^{-1} \times \log(2.01\ \mu M)$], respectively. The apparent coupling free energy of the binding of 9-AP is -1.1 kcal mol^{-1} ($\Delta\Delta G = \Delta G_2 - \Delta G_1$) and appears as a negative slope in Figure 8, which is consistent with positive cooperativity where the binding of the second 9-AP is favored over the first.

From the simulation of TST binding to $P450_{eryF}$, the $K_S = 286\ \mu$M and $\alpha K_S = 795\ \mu$M were extracted for the first and second binding, respectively. The ΔG, in this case, is -4.9 kcal mol^{-1} [$\Delta G_1 = 1.376$ kcal mol$^{-1} \times \log(286\ \mu M)$] for the first binding event and -4.3 kcal mol^{-1} [$\Delta G_2 = 1.376$ kcal mol$^{-1} \times \log(795\ \mu M)$] for the second. The apparent coupling free energy for the binding of TST is $+0.6$ kcal mol^{-1} ($\Delta\Delta G = \Delta G_2 - \Delta G_1$) and appears as a positive slope in Figure 8, which is consistent with negative cooperativity and shows that the second binding is disfavored over the first. In contrast, CYP3A4 shows an apparent coupling free energy for TST of $+1.78$ kcal mol^{-1}, which is shown in Figure 8 for a comparison (note the larger positive slope) (*18*).

While no firm conclusions could be made about the number of binding modes of the second 9-AP molecule by NMR, the X-ray crystal structure of 9-AP bound to $P450_{eryF}$ suggests that there is essentially only a single binding mode for the second 9-AP (*5*). Otherwise, the second 9-AP would appear completely disordered in the X-ray crystal structure. The single binding mode of 9-AP versus the multiple binding modes of TST suggests the intriguing possibility that there may be a relationship between the coupling free energy, a measure of cooperativity, and the number of binding modes. This relationship can be expressed quantitatively in terms of the differences in the coupling free energy. The coupling free energy determined for 9-AP and TST was -1.1 and $+0.6$ kcal mol^{-1}, respectively. The difference in the coupling free energy is 1.7 kcal mol^{-1} between 9-AP and TST, which represents a $\sim$20-fold difference in cooperativity [$10^{(1.7\ \text{kcal mol}^{-1}/1.376\ \text{kcal mol}^{-1})}$]. We propose that the 9-AP closest to the heme, being strongly coupled to the second 9-AP, shifts the distal 9-AP into a discrete binding mode, leading to tighter binding for the distal 9-AP. Assuming that TST binds similar to androstenedione in the X-ray crystal structure of $P450_{eryF}$ (*5*), the TST closest to the heme, being only weakly coupled to the distal TST, can only partially shift the TST into a discrete binding mode because of other competing binding modes, leading to weaker apparent binding for the second TST.

SUPPORTING INFORMATION AVAILABLE

An expansion of Figure 5 denoted as Figure S1 and values used for Figure 7 tabulated in Tables S1 and S2. This material is available free of charge via the Internet at http://pubs.acs.org.

REFERENCES

1. Pintacuda, G., Hohenthanner, K., Otting, G., and Muller, N. (2003) Angular dependence of dipole−dipole-Curie-spin cross-correlation effects in high-spin and low-spin paramagnetic myoglobin, *J. Biomol. NMR 27*, 115−132.
2. Ortiz de Montellano, P. R. (2004) *Cytochrome P450: Structure, Mechanism, and Biochemistry*, 3rd ed., Plenum Publishing, New York.
3. Atkins, W. M., Wang, R. W., and Lu, A. Y. (2001) Allosteric behavior in cytochrome p450-dependent *in vitro* drug−drug interactions: A prospective based on conformational dynamics, *Chem. Res. Toxicol. 14*, 338−347.
4. Atkins, W. M., Lu, W. D., and Cook, D. L. (2002) Is there a toxicological advantage for non-hyperbolic kinetics in cytochrome P450 catalysis? Functional allostery from "distributive catalysis", *J. Biol. Chem. 277*, 33258−33266.
5. Cupp-Vickery, J., Anderson, R., and Hatziris, Z. (2000) Crystal structures of ligand complexes of $P450_{eryF}$ exhibiting homotropic cooperativity, *Proc. Natl. Acad. Sci. U.S.A. 97*, 3050−3055.
6. Mitani, F., and Horie, S. (1969) Studies on P-450. 5. On the substrate-induced spectral change of P-450 solubilized from bovine adrenocortical mitochondria, *J. Biochem. 65*, 269−280.
7. Gillette, J. R., Darbyshire, J. F., and Sugiyama, K. (1994) Theory for the observed isotope effects on the formation of multiple products by different kinetic mechanisms of cytochrome P450 enzymes, *Biochemistry 33*, 2927−2937.
8. Banci, L., Bertini, I., Eltis, L. D., and Pierattelli, R. (1993) Spectroscopic characterization of a newly isolated cytochrome P450 from *Rhodococcus rhodochrous*, *Biophys. J. 65*, 806−813.
9. Banci, L., Bertini, I., Marconi, S., Pieratelli, R., and Sligar, S. G. (1994) Cytochrome P450 and aromatic bases: A ^{1}H NMR study, *J. Am. Chem. Soc. 116*, 4866−4873.
10. Pochapsky, S. S., Pochapsky, T. C., and Wei, J. W. (2003) A model for effector activity in a highly specific biological electron-transfer complex: The cytochrome $P450_{CAM}$−putidaredoxin couple, *Biochemistry 42*, 5649−5656.
11. Davydov, D. R., Kumar, S., and Halpert, J. R. (2002) Allosteric mechanisms in P450eryF probed with 1-pyrenebutanol, a novel fluorescent substrate, *Biochem. Biophys. Res. Commun. 294*, 806−812.
12. Davydov, D. R., Botchkareva, A. E., Kumar, S., He, Y. Q., and Halpert, J. R. (2004) An electrostatically driven conformational transition is involved in the mechanisms of substrate binding and cooperativity in cytochrome P450eryF, *Biochemistry 43*, 6475−6485.
13. Khan, K. K., Liu, H., and Halpert, J. R. (2003) Homotropic versus heterotopic cooperativity of cytochrome P450eryF: A substrate oxidation and spectral titration study, *Drug Metab. Dispos. 31*, 356−359.
14. Khan, K. K., He, Y. A., He, Y. Q., and Halpert, J. R. (2002) Site-directed mutagenesis of cytochrome P450eryF: Implications for substrate oxidation, cooperativity, and topology of the active site, *Chem. Res. Toxicol. 15*, 843−853.
15. Lewis, D. F. V. (2001) *Guide to Cytochromes P450: Structure and Function*, Taylor and Francis, New York.
16. Guengerich, F. P. (1995) Human cytochrome P450 enzymes, in *Cytochrome P450: Structure, Mechanism, and Biochemistry* (Ortiz de Montellano, P. R., Ed.) Plenum, New York.
17. Xiang, H., Tschirret-Guth, R. A., and Ortiz de Montellano, P. R. (2000) An A245T mutation conveys on cytochrome P450eryF the ability to oxidize alternative substrates, *J. Biol. Chem. 275*, 35999−36006.
18. Roberts, A. G., Campbell, A. P., and Atkins, W. M. (2005) The thermodynamic landscape of testosterone binding to cytochrome P450 3A4: Ligand binding and spin state equilibria, *Biochemistry 44*, 1353−1366.
19. Baas, B. J., Denisov, I. G., and Sligar, S. G. (2004) Homotropic cooperativity of monomeric cytochrome P450 3A4 in a nanoscale native bilayer environment, *Arch. Biochem. Biophys. 430*, 218−228.
20. Cupp-Vickery, J. R., Li, H., and Poulos, T. L. (1994) Preliminary crystallographic analysis of an enzyme involved in erythromycin biosynthesis: Cytochrome $P450_{eryF}$, *Proteins: Struct., Funct., Genet. 20*, 197−201.

21. Jefcoate, C. R. (1978) Measurement of substrate and inhibitor binding to microsomal cytochrome P-450 by optical-difference spectroscopy, *Methods Enzymol. 52*, 258−279.
22. Hildebrandt, A., Remmer, H., and Estabrook, R. W. (1968) Cytochrome P-450 of liver microsomes—One pigment or many, *Biochem. Biophys. Res. Commun. 30*, 607−612.
23. Omura, T., and Sato, R. (1964) The carbon monoxide-binding pigment of liver microsomes. 2. Solubilization, purification, and properties, *J. Biol. Chem. 239*, 2379−2385.
24. Jung, C., Ristau, O., and Rein, H. (1991) The high-spin/low-spin equilibrium in cytochrome P-450—A new method for determination of the high-spin content, *Biochim. Biophys. Acta 1076*, 130−136.
25. Delaglio, F., Grzesiek, S., Vuister, G. W., Zhu, G., Pfeifer, J., and Bax, A. (1995) NMRPipe: A multidimensional spectral processing system based on UNIX pipes, *J. Biomol. NMR 6*, 277−293.
26. Kay, L., Keifer, E. P., and Saarinen, T. (1992) Pure absorption gradient enhanced heteronuclear single quantum correlation spectroscopy with improved sensitivity, *J. Am. Chem. Soc. 114*, 10663−10665.
27. Mendes, P., and Kell, D. (1998) Non-linear optimization of biochemical pathways: Applications to metabolic engineering and parameter estimation, *Bioinformatics 14*, 869−883.
28. Mendes, P. (1997) Biochemistry by numbers: Simulation of biochemical pathways with Gepasi 3, *Trends Biochem. Sci. 22*, 361−363.
29. Mendes, P. (1993) GEPASI: A software package for modelling the dynamics, steady states, and control of biochemical and other systems, *Comput. Appl. Biosci. 9*, 563−571.
30. Dawson, J. H., Andersson, L. A., and Sono, M. (1982) Spectroscopic investigations of ferric cytochrome P-450−CAM ligand complexes. Identification of the ligand trans to cysteinate in the native enzyme, *J. Biol. Chem. 257*, 3606−3617.
31. Bertini, I., Luchinat, C., and Piccioli, M. (2001) Paramagnetic probes in metalloproteins, *Methods Enzymol. 339*, 314−340.
32. Davydov, D. R., Halpert, J. R., Renaud, J. P., and Hui Bon Hoa, G. (2003) Conformational heterogeneity of cytochrome P450 3A4 revealed by high-pressure spectroscopy, *Biochem. Biophys. Res. Commun. 312*, 121−130.
33. Cupp-Vickery, J. R., Garcia, C., Hofacre, A., and McGee-Estrada, K. (2001) Ketoconazole-induced conformational changes in the active site of cytochrome $P450_{eryF}$, *J. Mol. Biol. 311*, 101−110.
34. Cupp-Vickery, J. R., and Poulos, T. L. (1995) Structure of cytochrome P450eryF involved in erythromycin biosynthesis, *Nat. Struct. Biol. 2*, 144−153.
35. Hajduk, P. J., Dinges, J., Miknis, G. F., Merlock, M., Middleton, T., Kempf, D. J., Egan, D. A., Walter, K. A., Robins, T. S., Shuker, S. B., Holzman, T. F., and Fesik, S. W. (1997) NMR-based discovery of lead inhibitors that block DNA binding of the human papillomavirus E2 protein, *J. Med. Chem. 40*, 3144−3150.
36. Meyer, B., and Peters, T. (2003) NMR spectroscopy techniques for screening and identifying ligand binding to protein receptors, *Angew. Chem. 42*, 864−890.
37. Segel, I. H. (1975) *Enzyme Kinetics: Behavior and Analysis of Rapid Equilibrium and Steady-State Enzyme Systems*, John Wiley and Sons, Inc., New York.
38. Feeney, J., Batchelor, J. G., Albrand, J. P., and Roberts, G. C. K. (1979) The effects of intermediate exchange processes on the estimation of equilibrium constants by NMR, *J. Magn. Reson. 33*, 519−529.
39. Günther, H. (1980) The influence of dynamic effects on nuclear magnetic resonance spectra, in *NMR Spectroscopy: An Introduction* (Günther, H., Ed.) Chapter 8, Wiley, New York.
40. Binsch, G. (1967) The study of intramolecular rate processes by dynamic nuclear magnetic resonance, in *Topics in Stereochemistry* (Allinger, N. L., Eliel, E. L., and Denmark, S. E., Eds.) John Wiley and Sons, New York.
41. Lian, L. Y., Barsukov, I. L., Sutcliffe, M. J., Sze, K. H., and Roberts, G. C. (1994) Protein−ligand interactions: Exchange processes and determination of ligand conformation and protein−ligand contacts, *Methods Enzymol. 239*, 657−700.
42. Wemmer, D. E., and Williams, P. G. (1994) Use of nuclear magnetic resonance in probing ligand−macromolecule interactions, *Methods Enzymol. 239*, 739−767.
43. Levitt, M. H. (2001) *Spin Dynamics: Basics of Nuclear Magnetic Resonance*, John Wiley and Sons, Ltd., New York.
44. Williams, P. A., Cosme, J., Vinkovic, D. M., Ward, A., Angove, H. C., Day, P. J., Vonrhein, C., Tickle, I. J., and Jhoti, H. (2004) Crystal structures of human cytochrome P450 3A4 bound to metyrapone and progesterone, *Science 305*, 683−686.
45. Yano, J. K., Wester, M. R., Schoch, G. A., Griffin, K. J., Stout, C. D., and Johnson, E. F. (2004) The structure of human microsomal cytochrome P450 3A4 determined by X-ray crystallography to 2.05 Å resolution, *J. Biol. Chem. 279*, 38091−38094.

BI0518895